Volume 40
Number 7
July 2025
Pages 1605–1864

JAAS

Journal of Analytical Atomic Spectrometry

rsc.li/jaas

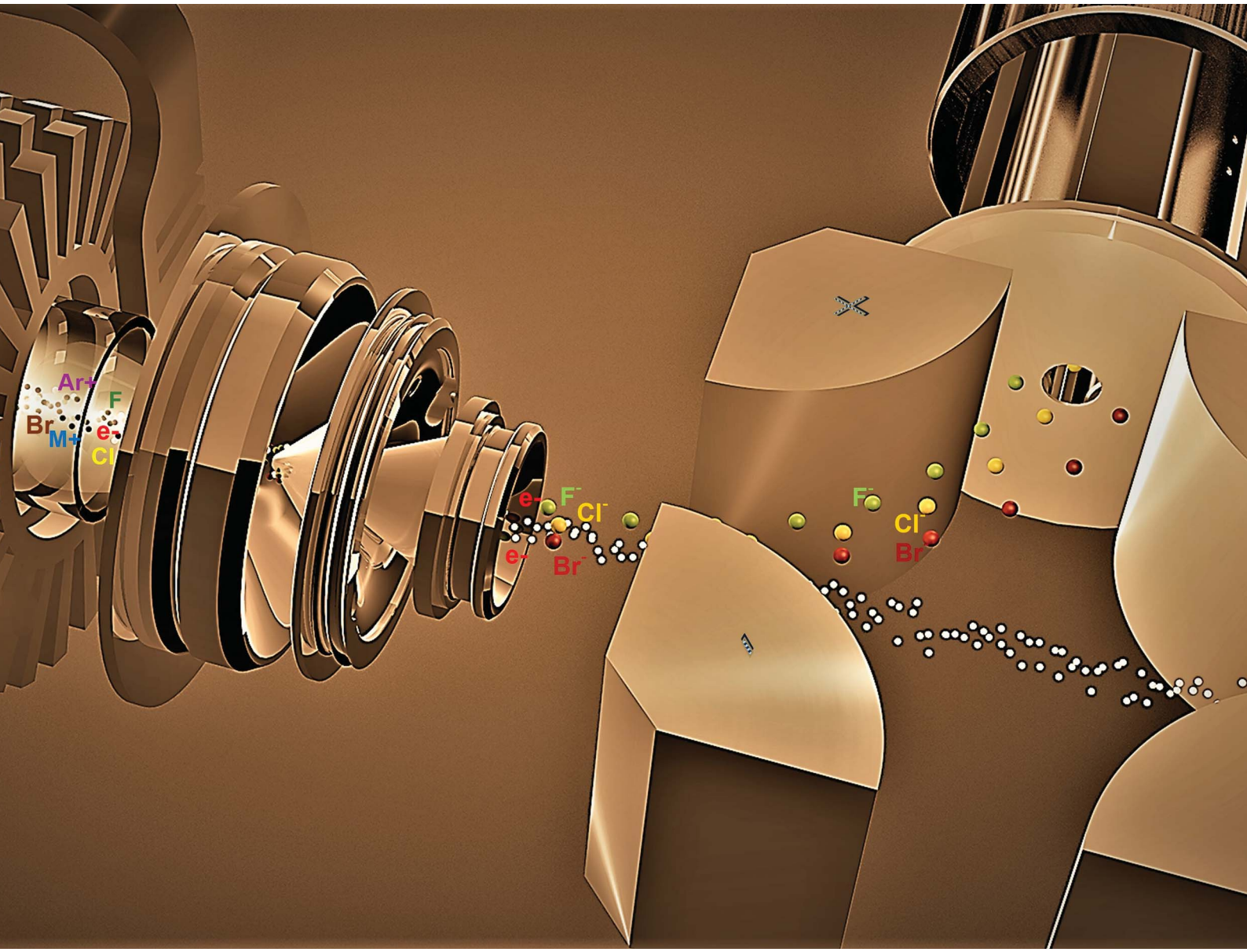

ISSN 0267-9477

ROYAL SOCIETY OF CHEMISTRY

PAPER

Andrea Raab, Hamid Badiei and Jörg Feldmann

How are negative ions in an ICPMS formed?

JAAS

PAPER

View Article Online
View Journal | View Issue

Cite this: *J. Anal. At. Spectrom.*, 2025, **40**, 1689

How are negative ions in an ICPMS formed?†

Andrea Raab, [a] Hamid Badiei[b] and Jörg Feldmann [a]

Interest in the determination of halogen containing compounds, especially fluorine, has increased exponentially over the last decade. Nevertheless, the development of instruments and methodologies for direct determination of fluorine has not yet reached a state where this is possible in routine laboratories. We revisited negative ion ICPMS using a modern commercial ICPMS with few modifications to the detector and ion optics to test whether fluorine detection with reasonable sensitivity would be possible with such an instrument. The aim of the study was to identify the processes behind the production of negative ions in a commercially available ICPMS. Using all halogens as diagnostic tools, many parameters such as water content, forward power, gas flows, and ion optics parameters were studied. Negatively charged bromine, chlorine and fluorine ions are generated in the interface, not the plasma, and their sensitivities mainly depend on the atomic radius (as a proxy for collision cross-section) and not on electron affinity. This knowledge is important for potentially building an instrument capable, among other elements, of determining fluorine with the capability to address the needs in environmental and medical science.

Received 2nd December 2024
Accepted 7th May 2025

DOI: 10.1039/d4ja00433g

rsc.li/jaas

1. Introduction

Organo-halogens, especially fluorinated compounds, are receiving increasing attention due to their widespread use in pharmaceuticals, agricultural compounds and industrial applications.[1] Most poly- or fully halogenated compounds are known to be persistent organic pollutants (POPs). They are known for their amphiphilic properties and chemical inertness. Nearly every industrial application involves one or several of them, whether during production or as part of the final product. Non-stick cookware and water-proof textiles are among the best-known public examples of their use. Drugs, herbicides or pesticides also often contain fluorine[2] or chlorine.[3] Certain PFAS exposures are linked to detrimental health effects such as cancer, infertility *etc.*[4–6]

The analytical problem is, however, that about 12 000 PFAS exist and fewer than 100 can reliably be determined with current analytical techniques based on molecular mass spectrometry. Techniques for the direct determination of halogenated compounds range from compound specific mass spectrometry to direct determination of the bound halogens.[7] Combining both approaches has shown that compound specific determination alone is not sufficient to achieve complete mass balance.[7–9]

Currently, molecular mass spectrometry is the main technique for the analysis of organo-halogens. However, compound-dependent sensitivity of the technique complicates instrument calibration for quantitative analysis of newly identified compounds with no available compound-specific standard. In most publications reporting halogenated compound concentrations, HPLC-triple-quad MS (ESI-MS/MS),[8,10] GC-MS[11,12] or GC-ECD (electron-capture detection) are used for the separation and detection of halogenated compounds.

Recently, interest in the determination of intrinsic element tags has increased, along with the drive to develop techniques enabling the detection of low halogen concentrations.[13] One of the techniques used for the direct determination of halogens is combustion ion chromatography (CIC), especially for fluorine-containing compounds.[8] With CIC, halogen-containing compounds are broken down to the halogen using hydropyrolysis.[14] These are then determined conductometrically as anions after separation. Determination of individual halogenated compounds is cumbersome since fractions from an HPLC-separation must be collected and individually measured for the presence of halogen. Continuum-source-high-resolution-graphite furnace molecular absorption spectrometry (HR-GFMAS) is another technique suitable for the same type of samples as CIC with similar limitations.[15–17] In this case detection of the halogen occurs *via* molecule-formation in the atomic cloud of the graphite furnace and detection of the MX (CaF or GaF) molecular absorption.

Positive ion ICPMS/MS (pICPMS) can be used for fluorine detection using a similar workaround as HR-GFMAS to overcome the low ionisation efficiency of fluorine in argon plasma and the high background of H_3O^+ on m/z 19.[18,19] For this barium

[a]*NAWI Graz, Institute of Chemistry, Analytical Chemistry - TESLA, University of Graz, Universitätsplatz 1, 8010 Graz, Austria. E-mail: andrea.raab@uni-graz.at*
[b]*PerkinElmer Scientific Canada ULC, 501 Rowntree Dairy Road, Woodbridge, Ontario, L4L 8H1, Canada*

† Electronic supplementary information (ESI) available. See DOI: https://doi.org/10.1039/d4ja00433g

is used with a special instrumental set-up. BaF^+ is formed in the plasma or post-plasma, although the exact location is not yet known. BaF^+ is separated in the reaction cell using oxygen or ammonia from $BaOH^+$, $BaOH_2^+$ and other molecular interferences before detection at m/z 157 (BaF^+) or 208 ($BaF(NH_3)_3^+$) depending on the reaction gas used.[18,20] Bromine and iodine are directly determined by pICPMS, whereas chlorine suffers from molecular interferences which can be overcome using H_2 in the reaction cell and a mass shift of 2.[21] Single quadrupole pICPMS has been tried for fluorine with little success.[22,23] High-resolution pICPMS can remove the water interference from fluorine but is not applied extensively to the determination of fluorine or other halogens.[24]

Various other plasma-based techniques have also been explored with a focus on fluorine determination: electrothermal vaporisation coupled with pICPMS[25] or ICPOES,[26] indirect determination of fluorine by pICPMS[27] and helium-microplasmas (MW(He)-plasma) combined with GC.[28,29] Atmospheric pressure plasma assisted reaction chemical ionization (PARCI) utilises an argon plasma for atomisation combined with a post-plasma reaction with a cation (sodium, barium and scandium were tried). The resulting molecular ion(s) are then determined with a mass spectrometer.[30,31] The instrumentation is still under development in one working group and at the moment utilised an Orbitrap-MS or a triple quadrupole MS as the detector in positive mode for the reaction products.[32]

Fig. 1 gives an overview of the achievable instrumental detection limits (DLs) for various techniques for fluorine and fluorinated compounds. For all of them, the DL depends also strongly depends on background contamination. GC-MS and ESI-MS/MS can be considered as the most sensitive techniques for compound specific detection, as shown in Fig. 1, even without the usually performed sample preconcentration. Considering, for example, the DL for PFOS of ~1.5 ng L^{-1} (~0.003 nM), this would be equivalent to about 1 ng F per L, which would be the DL an elemental method has to achieve to compete with molecular methods for easily ionised compounds. For partially fluorinated compounds the elemental DL would have to be even lower for direct determination. So far, all elemental methods, despite the progress made, still lack sensitivity compared to molecular techniques.

One alternative for the determination of halogens by plasma-based techniques has not recently been considered. This is negative ion ICPMS (nICPMS). Early research work in this area was limited to only a few publications shortly after the introduction of the first commercially available ICPMS.[33–35] At that time detection limits of about 110 μg L^{-1} for fluorine,[34] 0.75–1 μg L^{-1} for chlorine[34,36] and 2 μg L^{-1} for bromine[34] were estimated. Except for one theoretical work, nICPMS[37] has not been studied for more than 35 years. During this time the performance of pICPMS has improved greatly.

The aim of this study was to modify a modern-day pICPMS instrument (NexION® 2000) for the detection of negative ions with minimal hardware changes. The aim of the current study was three-fold: firstly, to further investigate the ionization mechanism of negatively charged ions and their transmission into the mass spectrometer and secondly, to explore the effect of ICPMS operating conditions on analytical performance characteristics and figures of merit of the system with a focus on halogens, and finally, to demonstrate the capabilities of the system through the analysis of total fluorine in real samples with tea leaves as an example. The focus of the study was fluorine, since it is, the most difficult halogen to detect by elemental methods. Other halogens were monitored to understand the ionisation processes.

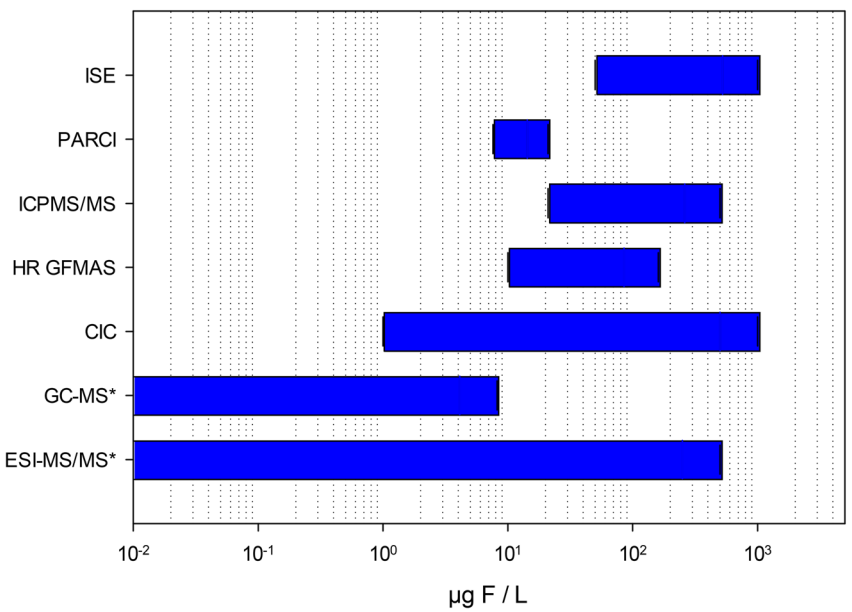

Fig. 1 Estimated instrumental detection limits for fluorine (*: fluorinated compounds) taken from various literature sources; ESI-MS/MS, GC-MS and PARCI data from flow injection or in combination with a separation technique; for chlorine and bromine detection limits are similar except for ICPMS/MS where they are lower (est. 0.01–0.1 μg L^{-1}). Table S2† shows some additional detection limits for F, Cl and Br from the literature.

2. Experimental

2.1. Instrument

The instrument used was a NexION® 2000 (PerkinElmer Inc., Shelton, CT, USA). The only modification needed to study nICPMS and its capabilities with special emphasis on fluorine detection is the replacement of the detector and its associated power supply boards (Fig. 2). The detector power supply was modified to provide a sufficient positive bias voltage range, and the original simultaneous pulse/analog detector was replaced with a single pulse-stage discrete dynode detector with a gain of up to 5×10^7 and a pulse range of up to 3×10^7 counts per second. All other electronic components of the instrument, notably the quadrupole drivers and electrostatic lenses (in this case also in a quadrupole arrangement, QID), are bipolar and can operate under both positive or negative voltages as needed. In-instrument parts made of Teflon were changed as far as possible to polyethylene materials. Interface gate seals were also changed to the ones made from silicon and the grease used was changed to fluorine-free material. The instrument was equipped with standard nickel cones (sampler, skimmer (aperture ID 0.6 mm), and hyperskimmer), a Peltier-cooled cyclonic spray chamber (set to 0 °C), a Meinhard-glass nebulizer and a standard Fassel-type torch with an injector ID of 1.5 mm.

2.2. Chemicals

All chemicals used were of analytical grade. Water used throughout the experiments was freshly prepared using a MilliQ-system (Merck, Germany). Elemental standards for halogens were ion-chromatography standards (1000 mg L^{-1}) obtained from Roth, Austria. A working stock solution containing halogen ions (F, Cl, Br and I) at 10 mg L^{-1} or other concentrations as required was prepared in water. The blank solution was pure water. For tuning purposes, a 10 mg L^{-1} mixed solution all halogen ions in water (referred to as 10 mg Hal per L) and a water blank were used. Deuterium oxide (99.98%) and water-^{18}O (97%) were both obtained from Deuteron (Germany).

As test samples, black tea (bought in Graz 2022) and a tea reference material (F: 320 ± 31 mg kg^{-1}, GBW07605 GSEV-4, China) were used. Extracts of tea (1 to 2 g/50 mL) were prepared by infusion with boiling water for 6 min followed by centrifugation. For measurement the samples were diluted 1 + 4 with water. All samples were also spiked with one and two mg F per L to determine spike recovery.

2.3. Ion-selective electrodes (ISEs)

For quality control of the tea results, an ISE was used with TISAB IV in addition to the reference material. TISAB IV was prepared by dissolving 4.0 g of CDTA (*trans*-1,2-diaminocyclohexan-*N*,*N*,*N*′,*N*′-tetraessigsäure monohydrate) in 500 mL of water. 57 mL glacial acetic acid and 58 g sodium chloride were added to the solution and mixed well. After cooling to room temperature, the pH was adjusted to 5.5 with 5 M sodium hydroxide and the solution was made up to 1 L with de-ionized water. The 1 + 4 diluted tea extracts were mixed 1 + 1 with TISAB IV. The electrode used was an Orion Ionplus sure-flow/fluoride electrode from Thermo Scientific (Germany) with an integrated reference electrode and a voltameter (Orion 5 Star, Thermo Scientific, Germany). External calibrations were used to calculate the concentrations.

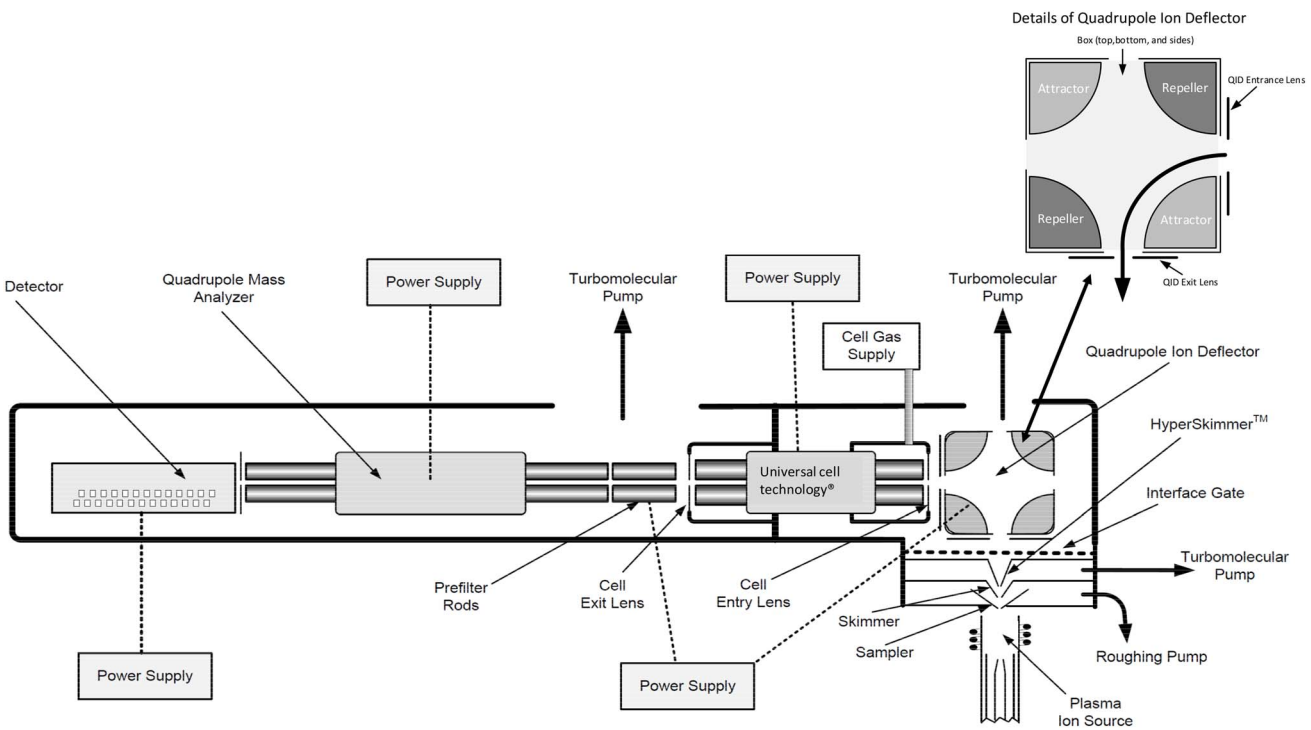

Fig. 2 Instrument set-up Nexion2000®.

2.4. Calculations

The signal to blank ratio was calculated by dividing the signal of the 10 mg L^{-1} standard by the blank signal.

To estimate the maximum contribution of $^{18}O^{1}H^{-}$ at m/z 19, the ratio of m/z 17/16 was calculated without considering the contribution of $^{17}O^{-}$ to the signal at m/z 17 (eqn (1)). To estimate a lower boundary for the OH^{-} contribution, first the contribution of $^{17}O^{-}$ to the signals at m/z 17 and m/z 18 was estimated based on the signal at m/z 16 eqn (2a–d).

$$\%\ \mathrm{OH} = \left(\left[I_{m/z18} \times \frac{m/z17}{m/z16}\right] \times 100\right) \Big/ I_{m/z19} \quad (1)$$

$$I^{^{17}\mathrm{O}} = I_{m/z16} \times 0.038/99.8 \quad (2a)$$

$$\left(\frac{m/z17}{m/z16}\right)_{\text{corrected}} = \left(I_{m/z17} - I^{^{17}\mathrm{O}}\right) \Big/ I_{m/z16} \quad (2b)$$

$$I^{^{18}\mathrm{O,corr}} = I_{m/z18} - \left(I^{^{17}\mathrm{O}} \times \left(\frac{m/z17}{m/z16}\right)_{\text{corrected}}\right) \quad (2c)$$

$$\%\mathrm{OH}_{\mathrm{corr}} = \left(\left[I_{m/z^{18}\mathrm{O,corr}} \times \frac{m/z17}{m/z16}, \mathrm{corr}\right] \times 100\right) \Big/ I_{m/z19} \quad (2d)$$

The influence of $^{17}O^{2}D^{-}$ on the signal is minimal and neglected.

The limit of determination was estimated as follows:

$$\mathrm{DL} = \text{standard error of regression} \times 3.3/\text{slope}$$

3. Results

The instrument parameters were first set roughly by estimation to achieve some sensitivity for negative halogen ions by applying positive polarity to the QID (electro-static lenses in quadrupole arrangement), CRO (cell rod off-set), QRO (quadrupole rod off-set) and cell entrance/exit (see instrument settings, Table 1) before performing a thorough tuning of each individual parameter. The mass calibration parameters were kept unchanged from those used in the positive-ion mode. The torch position was centred on the sampler aperture with a standard sampling depth of 11 mm. In individual experiments specific parameters and their influence on the fluorine signal at m/z 19 and other ions were tested. The optimal setting of a specific parameter was then carried over to the next parameter tested. The parameters were tested in the order shown in Table 1.

3.1 Mass scans in nICPMS: signals and their identification

3.1.1 Background. Scanning the mass range from 1 to 150 m/z (Fig. 3) showed a background signal of about 1500 cps per mass. This is comparable to the background determined by Fulford *et al.* with an Elan250.[34] The orthogonal ion path of the NexION® 2000 therefore showed no improvement. The origin of the background is currently unknown and is a subject of future investigation. Chtaib *et al.* concluded that, unlike pICPMS, nICPMS has inherently a higher background since free electrons produced in the plasma are not stopped from reaching the detector.[35] Whether the increased background originates from electrons reaching the detector is currently unknown.

3.1.2. Blank (MilliQ-water). A mass scan of water (Fig. 3a–c, red line) showed significant signals at m/z 16 to 19 and 32 and other signals particularly at m/z 35, 37, 79 and 81. The latter signals are attributed to chlorine and bromine contamination. Canulescu *et al.* also detected strong signals of F^{-}, Cl^{-}, Br^{-}, and NO_2^{-} (among others) in pure platinum foil using a pulsed glow discharge instrument (GD-TOFMS in negative mode).[38] Halogen background ions seem to be widespread independent of matrix measured. In contrast to the findings of Fulford *et al.* the signals at m/z 40 (argon $Ar^{+/-}$) and m/z 46 (NO_2^{-}) were relatively low whereas NO^{-} (m/z 30) was not detectable.[34] The high background observed at m/z 19 can be the result of molecular interferences from water or fluorine contamination (for details see Origin of background at m/z 19).

3.1.3 Element standard. In a mixed standard solution containing 10 mg Hal per L, halogen signal intensities decreased in the order of Cl > Br > I > F (Fig. 3a–c, blue line). Beside the isotopes of the elements, ClO^{-}, BrO^{-} and IO^{-} were also present (Fig. 3b and c). Chlorine seems to form about 1 ± 0.1% ($n = 4$) of ClO^{-}, while bromine forms 2 ± 0.15% BrO^{-} ($n =$

Table 1 Typical settings for nICPMS and pICPMS

	Negative mode	Positive mode (typical settings)
Nebulizer gas flow (L min^{-1})	0.85	1.0
Auxiliary gas flow (L min^{-1})	0.85	1.2
Plasma gas flow (L min^{-1})	15	16
Forward power (W)	1600	1600
CRO (V)	+10	−6
QRO (V)	+12	0
Cell entrance/exit (V)	+19.5	−12
QID attractor (V)	+110	−100
QID box (V)	+68.5	−40
QID entrance (V)	+41.5	−25
QID repellor (V)	+12.5	−12
Detector (V)	+890 (first dynode), +3060 (final dynode)	−2000 (first dynode), +1000 (final dynode)
Detector gain (V)	2170	3000
Discriminator	20	12

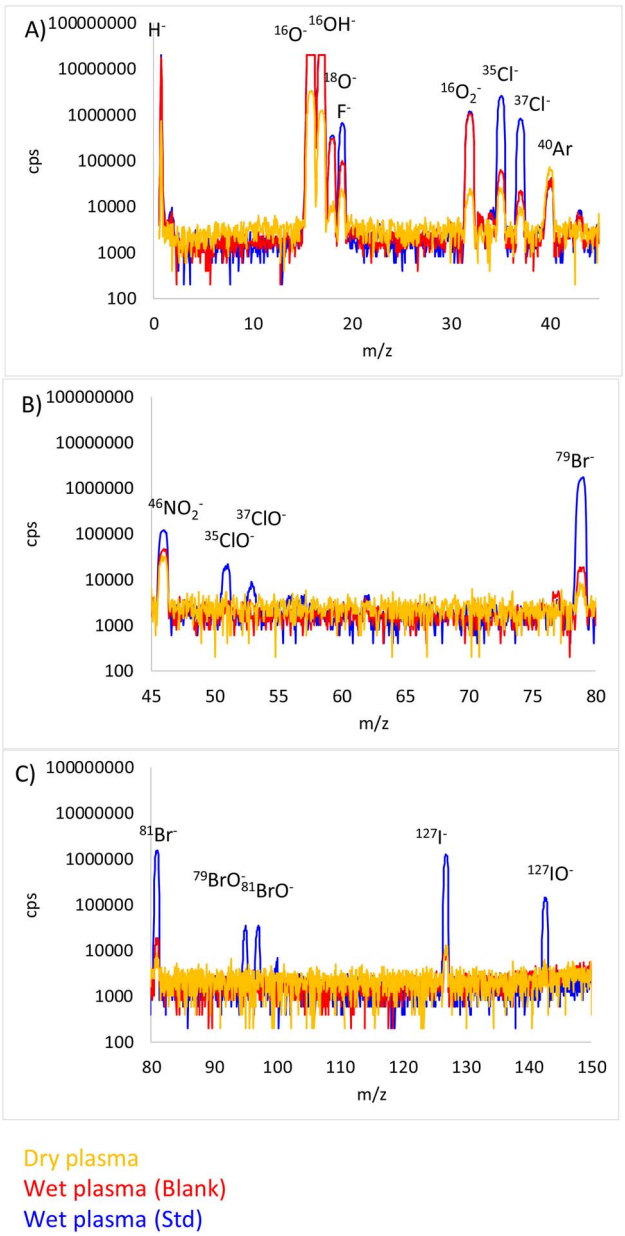

Fig. 3 a–c) Full mass scan under dry and wet plasma conditions; other parameters were identical, showing the region between m/z 1 and 150 (instrument settings similar to Table 1, detector voltage 755 and 2900 V); yellow line: no solution nebulized, red line = water, and blue line = 10 mg L^{-1} mixed halogen standard.

4) and iodine forms 16 ± 1% IO^- ($n = 4$). Chtaib *et al.*[35] were also able to detect the formation of ClO^-, but could not detect BrO^- when using a 3 M HCl solution containing 86 mg Br per L; whether this is instrument dependent or due to the use of a highly acidic solution is unclear. The tendency of oxide formation seems to be identical with the tendency in pICPMS using oxygen as the reaction gas (Cl < Br < I).[39] The occurrence of FO^- (m/z 35) cannot totally be excluded (due to the $^{35}Cl^-$ signal) but it does not contribute significantly to the m/z 35 signal since the 37/35 (chlorine) ratio of 0.33 ± 0.05 ($n = 4$) closely matches the theoretical ratio of 0.32 as is the measured isotope ratio of bromine (0.92 ± 0.2 *versus* 0.97 $n = 4$).

3.1.4 Dry plasma conditions. Under dry plasma conditions (*i.e.*, no solution nebulized, tubing for solution plugged, nebulizer gas on) the dominant signals were observed at m/z 16 to 19 followed by m/z 40. The mass scan (Fig. 3a–c, yellow line) also showed small signals for Cl^-, Br^- and I^- of unknown origin without the introduction of any solution.

3.2 Effect of instrument operating conditions on signal intensity

Signal intensities for halogen ions are highly dependent on instrument's operating conditions, with the nebulizer flow rate

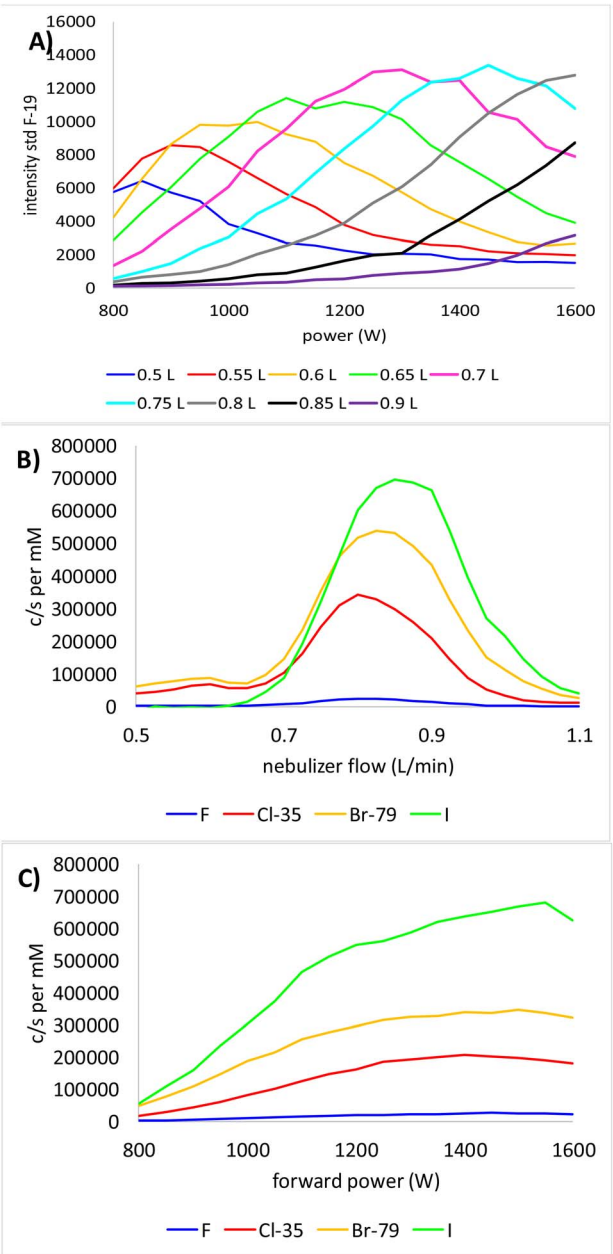

Fig. 4 A) An example of fluorine (m/z 19) intensity variation with forward power at set nebulizer gas flow rates; (B) signal intensity (in cps per mM Hal) *versus* nebulizer gas flow rate at 1600 W (C) signal intensity (in cps per mM Hal) *versus* forward power for a nebulizer gas flow rate of 0.8 L Ar per min (sample 10 mg L^{-1} halogen mix).

and forward power exerting the largest influence. These two parameters are found to be correlated (Fig. 4a for fluorine) and exhibit slight daily variations as observed in pICPMS. The relationship between nebulizer gas flow and forward power settings in nICPMS was already observed by Fulford *et al.* for chlorine.[34] In pICPMS the correlation between the nebuliser gas flow rate and forward power was studied early by Horlick *et al.* and is identical to the behaviour in nICPMS.[40] The main reason for the strong effect on signal intensity of both parameters lies in their influence on the atomisation/ionisation processes in the plasma. However, whether the reason for their impact on signal intensity in nICPMS is the same remains unknown at the moment (see also ionisation processes governing the abundance of negative ions in ICPMS). Auxiliary gas flow, electrostatic lens voltage (in case of the NexION® 2000 QID), QRO and CRO voltages do not vary significantly between days. Sampling depth had much less influence on sensitivity than in the BaF^+ method used in pICPMS where it has a significant influence on signal intensity.[41] This difference between the behaviour in nICPMS and pICPMS can be explained by the fact that for pICPMS the formation of Ba^{2+} plays an important role in the ability to form BaF^+, whereas in nICPMS no such influence is present. For data plots of these parameters including the estimated contribution of OH^- to *m*/*z* 19 see ESI Fig. S2–12.†

The four halogens behave nearly identical under all parameter settings when tuning is done for maximum intensity only. This is shown in Fig. 4b and c using nebulizer gas flow and forward power as examples. In all examples displayed in Fig. 4b and c, it is obvious that fluorine is the least sensitive of all four halogens (see also: ionisation processes governing the abundance of negative ions in ICPMS). This is especially clear after correcting the signal for molar concentration. Sensitivities and detection limits (DL) achievable with this modified NexION® 2000 are shown in Table 2. Compared to the results achieved by Bu *et al.*[24] using pICPMS at medium resolution, the DL for fluorine is significantly better and it is in the range of the DL achievable using the BaF^+-method with an average pICPMS/MS instrument.[18,20,42] Fulford *et al.* estimated a DL of 110 μg L^{-1} in nICPMS compared to the 400 μg L^{-1} estimated by Vickers *et al.*[33,34] In the current configuration the modified NexION® 2000 achieved a similar DL for fluorine with 54 μg L^{-1} (Table 2). For the other halogens the DLs achieved are comparable to the ones estimated by Vickers *et al.*,[33] but significantly higher than the DLs achieved by Bu *et al.*[24] The achievable DL for all halogens are strongly limited by blank levels.

The fluorine DL is well above what is needed for applications involving low fluorine content (*e.g.*, water samples), which also require a combination of HPLC-ICPMS and therefore likely have even higher DLs. To determine, for example, PFOS at a level of 0.1 μg L^{-1} (equivalent to the sum PFAS parameter required by the EU drinking water regulation)[43] an elemental detector would need a DL of below 0.06 μg F per L without employing sample preconcentration. For elemental detectors (and this is nearly independent of the detector used), a preconcentration factor of at least 2500 is required at the moment. One reason for this is that fluorine detection suffers from exceptionally high background counts (Table 2) (more about this can be found in origin of background at *m*/*z* 19) both in nICPMS and in all other methods.

3.3 Ionisation processes governing the abundance of negative ions in ICPMS

In pICPMS, ions are created in the plasma directly and the ionisation efficiency of elements is governed by their first ionisation potential. In pICP-MS, the ionization efficiency for most elements exceeds 90% due to their first ionization potentials being significantly lower than that of argon (15.67 eV) to form positive ions. Elements with the first ionization potential below 7 eV are fully ionized in the plasma. Bu *et al.* showed the linear relationship between sensitivity and the first ionisation potential clearly for the halogens using medium resolution pICPMS (Fig. 5a).[24] In nICPMS one could therefore expect electron affinity (EA) to be the governing factor producing negative ions in the plasma. Electron affinity is thermodynamically described as the energy generated, when an atom accepts an electron in the gas phase. In this case it would be expected that fluorine and bromine showed similar sensitivities and both should be slightly lower than those for chlorine.

Fig. 5b shows clearly that exactly the opposite is true. Iodine the element with the lowest electron affinity among the halogens is the most sensitive while fluorine behaves differently

Table 2 Typical measured count rates and estimated DLs compared to DLs from the selected literature ($DL^{33,34,45,46} = 3\sigma S/N$ and DL^{24} see Table 1)

	m/*z* 19 (F)	*m*/*z* 35 (Cl)	*m*/*z* 79 (Br)	*m*/*z* 127 (I)
Blank (cps)	4494	2002	1265	2922
10 mg L^{-1} standard (cps)	32 233	146 544	117 931	128 053
Ratio (std/blank)	7.2	73	93	43
cps/μg L^{-1} (blank subtracted)	2.8	15.5	12	10
DL μg L^{-1}	54	7	30	46
DL μg L^{-1} (ref. 34)	110	1	2	6
DL μg L^{-1} (ref. 33)	400	80	10	70
DL μg L^{-1} (ref. 24)	5070[a]	3.25[b]	0.08[b]	0.05[b]
DL μg L^{-1} (ref. 18, 20 and 44)	22–60			
DL μg L^{-1} (ref. 45)		1.4–1.6	0.8–1.5	
DL μg L^{-1} (ref. 46)				1

[a] In MR-mode. [b] In HR-mode.

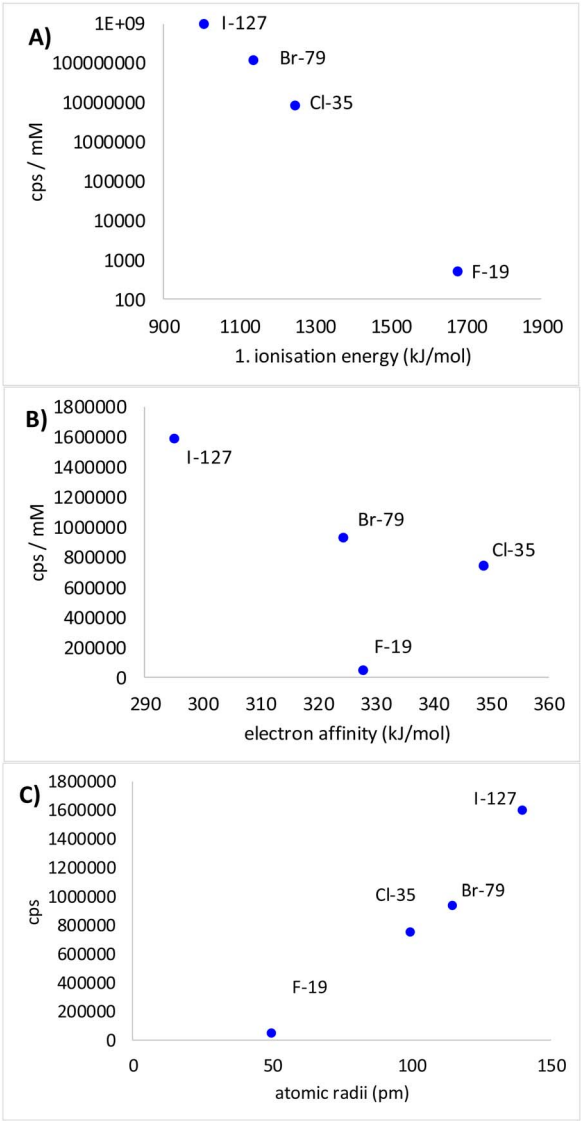

Fig. 5 Dependence of signal intensity on (A) ionization energy for medium resolution-pICPMS (data from Bu *et al.*[24]) and (B) (cps per mM isotope) electron affinity for nICPMS; (C) atomic radii for nICPMS and the dependence of signal intensity (cps per mM) on these parameters.

from the other three halogens. The production of negative halogen ions is therefore not primary depending on electron affinity (some electronic and physical properties of interest for halogen atoms are summarised in Table S1†). The EA is significantly lower than first ionisation potentials – for example, fluorine has an electron affinity of 3.5 eV – making the in-plasma formation of stable anions highly unlikely.[47] Estimates based on the Saha equation, as well as a NASA report,[48] suggest that stable fluorine anions can only form at temperatures below 3000 K, whereas the temperature in the central channel of the plasma exceeds 5000 K.

In the "afterglow" of the plasma (between the sampler and skimmer and behind the skimmer) the temperature drops rapidly (as *e.g.* modelled by Kivel *et al.*); therefore an electron attachment process in this region is more likely to lead to a stable negative ion.[49] Since we did not investigate the potential formation of a shockwave (= re-heating of particle beam) at the skimmer tip,[49–51] we are currently unable to distinguish whether formation occurs between the sampler and skimmer or behind the skimmer. Gas kinetic temperatures are below 3000 K in this regions, as determined by Lim *et al.*[52] and modelled by Kivel *et al.*[49] and Nagulin *et al.*[53] This would allow processes similar to those described for negative mode pulsed glow discharge to occur.[38,54] These processes have been identified as dissociative or non-dissociative electron attachment, ion pair formation during collisions,[54] charge transfer and/or Penning ionisation.[38] A major factor influencing the efficiency of ion formation in this case is the collisional cross-section of the atom in an electron capture process, which would first lead to the formation of an excited anion. Stoffels *et al.*[55,56] showed that an excited parent anion can stabilise by either (i) autodetachment (electron loss), (ii) deactivation of the excited state by photon emission or (iii) collision with a third particle (shown for collision with atomic hydrogen by Huels *et al.*[57]); stabilisation by dissociation is not applicable to atomic ions.[58] The first process is of no interest here since an atom is formed in this process. The third (non-dissociative electron attachment by two or three-body collisions) is the most likely reason for the formation of halogen anions. Some other non-resonant process like charge-transfer, might also occur. From the positive correlation between signal intensity and atomic radii (as a substitute parameter for the unknown collisional cross section), it seems that electron capture is the dominating factor for ionisation in nICPMS (Fig. 5c), a likely ionisation mechanism already suggested by Fulford *et al.*[34] From their measurements of the stopping potential they concluded that negative ions are not formed in the plasma itself, but are the result of post-plasma electron capture.[34]

When electron capture is the main ionisation process, the number of electrons (estimated at 10^{13} cm^{-3}),[59] residence time and their kinetic energy distribution in the interface region after the sampler will influence the efficiency of anion formation. The kinetic energy of electrons can be estimated from the electron temperature.[59] Electron temperature is affected by plasma conditions and sample composition differently than electron numbers.[59] Electron temperature does not drop in the interface region the same way as gas kinetic temperature.[59] Electron density after the sampler in contrast decreases with higher nebulizer gas flow and increases with forward power, but seems unaffected by the presence of matrix elements or water.[59] The signal variation during the optimisation of the forward power and nebulizer flow rate (Fig. 4) indicate that electron density is the more important parameter for successful electron capture.

Besides the formation rate of negative ions, their rate of loss, through collisions with cations, wall surfaces or in other ways, has an influence of the number of negative ions reaching the detector. Considering that for lighter ions, transmission rates in quadrupole ICPMS instruments are generally poorer than for heavier ones, transmission loss throughout the complete ion-path may be higher for fluorine compared to heavier halogens, thereby further degrading the achievable sensitivity. In addition, the smaller fluorine atom (compared to the other

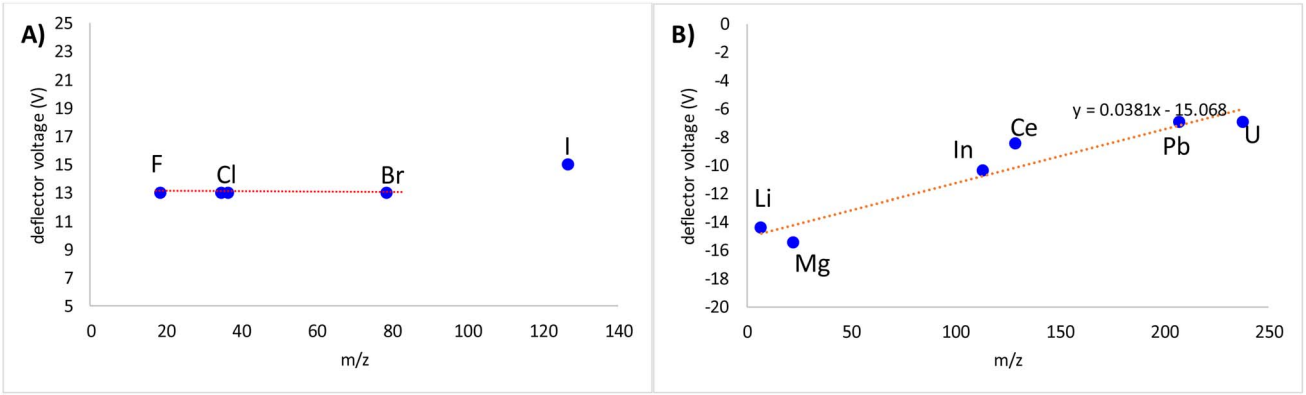

Fig. 6 Deflector voltage required for optimum signal intensity (A) nICPMS; (B) pICPMS 3.4 origin of background on *m/z* 19.

halogens) is less likely to interact with free electrons due to its small radius (Table S1†).

Another factor suggesting post-plasma ionisation of at least fluorine, chlorine and bromine is the similar kinetic energy these ions display during QID deflector optimisation (Fig. 6a). In pICPMS, the QID deflector voltage needed for best transmission into the quadrupole is mass dependent (Fig. 6b). For ions created in the plasma the kinetic energy with which they enter the interface region is similar. These ions travel with the velocity of the bulk argon as they travel through the interface region of the mass spectrometer and gain energy in the supersonic expansion region behind the sampler cone. In the absence of any other post interface extractive lenses and any significant plasma potential these energies typically range from 2–8 eV depending on the mass range.[60,61]

In nICPMS the required QID voltages for optimum transmission of fluorine, chlorine and bromine do not show a dependence on atomic mass (Fig. 6a) indicating different kinetic energies of the ions created in the "afterglow" of the plasma. This may indicate, that during the post-plasma electron attachment process required for anion formation, the concomitant loss of energy during anion stabilisation results in near identical velocities for the anions. Iodine is however an outlier showing an increased voltage requirement, which indicates that the kinetic energy (hence velocity) of iodine anions is different from the lighter halogens. It is possible that iodine anions are created at least partially by a different mechanism and are not only due to post-plasma electron capture.

3.4 Origin of background on *m/z* 19

The background signal at *m/z* 19 is another limiting factor for the sensitive determination of fluorine. The question is whether this background only originates from oxygen/water interferences or whether there is a background concentration of fluorine present in MilliQ water (or any other solution).

Potential interferences at *m/z* 19 are $^{18}O^{1}H^{-}$, $^{38}Ar^{2+/-}$, $^{1}H_3{}^{16}O^{-}$ (suggested by Vickers *et al.*[33]), $^{1}H_2{}^{17}O^{-}$ (suggested by Vickers *et al.*[33]), $^{17}O^{2}H^{-}$ or $^{16}O^{1}H^{2}H^{-}$. A potential ^{38}Ar interference at *m/z* 19 should also yield a very strong signal at *m/z* 20 ($^{40}Ar^{2+/-}$). This is not the case (Fig. 3 and 7). Therefore, an interference from Ar can be excluded. To decide, which molecular interferences originate from water full mass scans using different types of water (H_2O, D_2O, and $H_2{}^{18}O$) were measured. Due to restriction regarding the amount of solution ($H_2{}^{18}O$) available, these experiments were performed in a "semi-dry" set-up. In practice this meant adding small amounts of solution (~0.2 mL) to the base of the spray chamber *via* a syringe and replenishing this fluid as needed. The spray chamber, which is normally cooled to 0 °C, was heated to 30 °C to improve evaporation of the solutions in this experiment. The other instrument settings were the same as those used under wet plasma conditions. Between measuring the different types of water (H_2O, D_2O and $H_2{}^{18}O$), the plasma was run under dry conditions until signal stability was reached. Fig. 7 shows the spectra (*m/z* range between 15 and 25) of these measurements.

For the above-mentioned molecular interference of $^{1}H_3{}^{16}O^{-}$ to occur, D_2O should show a strong signal at *m/z* 22 and $H_2{}^{18}O^{-}$ a signal at *m/z* 21 (Fig. 7). At neither *m/z* a signal can be detected above the electronic background. Consequently, this molecule can be excluded from occurring. For the ion $^{1}H_2{}^{17}O^{-}$ to occur a signal at *m/z* 21 must be present using D_2O which is not the case. Using $H_2{}^{18}O$ does not show an additional signal at *m/z* 20 compared to D_2O or H_2O. Therefore, this molecular interference can be excluded as well to contribute to *m/z* 19 using "normal"

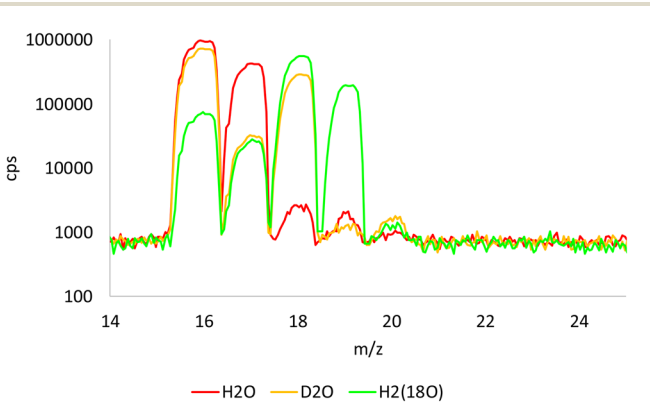

Fig. 7 Spectra of H_2O, D_2O, and $H_2{}^{18}O$. Scan from *m/z* 14 to 25.

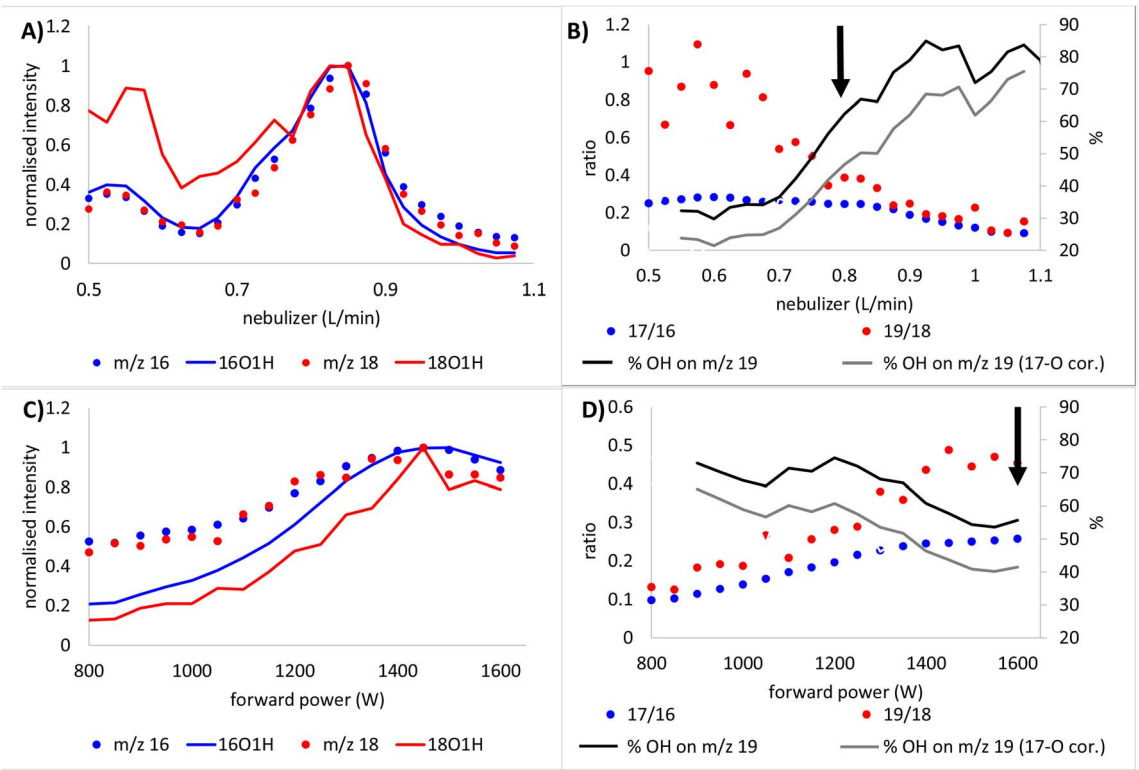

Fig. 8 (A) and (C) The dependence of signal intensity (blank solution) *vs.* (A) nebulizer gas flow rate (at forward power 1600 W) and (C) *vs.* forward power (at nebulizer gas flow rate of 0.8 L min^{-1}), panels (B) and (D) show the calculated ratios *m/z* 17/16 and *m/z* 19/18 plus the estimated relative contribution of OH to the signal at *m/z* 19 (max–min); eqn (1–2d) used for calculations; black arrow indicates the area of highest sensitivity.

water. The "only" molecular interference occurring using normal water at *m/z* 19 is therefore $^{18}O^{1}H^{-}$.

To estimate the amount of OH^{-}-formed compared to O^{-} the sensitivity of the detector was decreased so that *m/z* 16 and 17 were detectable without detector saturation in a standard setup. If the background at *m/z* 19 originates only from the formation of $^{18}O^{1}H^{-}$ than the ratio of *m/z* 17 ($^{17}O^{-}$ + $^{16}O^{1}H^{-}$) over *m/z* 16 ($^{16}O^{-}$) should be nearly identical to the ratio of *m/z* 19 ($^{18}O^{1}H^{-}$) over *m/z* 18 ($^{18}O^{-}$ + $^{17}O^{1}H^{-}$). As can be seen in Fig. 8a and b the nebulizer gas flow (respectively the amount of water reaching the plasma) is a major contributing factor to the amount of $^{18}O^{1}H^{-}$ at *m/z* 19 when it is set to values higher than those required for maximum signal intensity at *m/z* 19. At optimum signal intensity, $^{18}O^{1}H^{-}$ contribution is estimated to be between 50 and 65% to the signal of *m/z* 19, when water is aspirated. The applied forward power influences the amount of OH^{-} as well, but in this case the lower the power the higher the contribution of OH^{-} to the signal (Fig. 8c and d). At optimum forward power the contribution of $^{18}O^{1}H^{-}$ to *m/z* 19 was between 40 and 60%. Other instrumental parameters (QID, CRO, QRO, cell entrance/exit, sampling depth and auxiliary gas flow) had very little to no effect on the contribution of $^{18}O^{1}H^{-}$ to *m/z* 19 (Fig. S1–S10†). With a well optimised instrument about 50% of the blank signal on *m/z* 19 is of water origin. The rest of the signal is very likely the result of contamination with fluorine-containing compounds from the lab environment, the instrument and the gases. The high amount of fluorine contamination also explains the relatively large signal at *m/z* 19 observed under dry plasma conditions (Fig. 3).

3.5 Application: total fluorine in tea

Given the current sensitivity of the system in negative ion mode, it is of interest whether determination of fluorine in real samples would be possible. To this end, extracts of two different black tea samples and a tea reference material were prepared and measured using external calibration. The calibration curve was linear between 0.1 and 25 mg F per L (r^2 better than 0.993), while the DL of the day estimated from blanks (n = 10) was 0.12 mg F per L (DL estimated from regression of calibration was 0.06 mg F per L).

One of the samples (1) was extracted from the leaves (as is) and as finely ground material and the other (sample 2) was extracted at two different concentrations (1 respectively 2 g tea per 50 mL water). All samples were also spiked with two different concentrations of fluoride (1 and 2 mg F per L) to determine spike recovery. Sample 1 showed that the extraction efficiency of fluoride is influenced by particle size (Table 3). Finely ground samples are more effectively extracted using hot water than course samples. The system seems to react to the presence of other ions as can be seen comparing the two different matrix concentrations used for sample 2. This is also clear considering the higher spike recovery rate for sample 2 (2 g/50 mL). The CRM recovery was 85.7 ± 1.2%. The same solutions were also measured by ISE. Compared to ISE (the standard

Table 3 Fluorine content in tea leaves ($n = 3$)

	mg F^- per kg (ISE)	Spike recovery%	mg F per kg (ICPMS)	Spike recovery%	Difference ICPMS/ISE (%)
Sample 1 (leave)	170 ± 1.4	98 ± 2.1	202 ± 3.2	105 ± 1.5	119
Sample 1 (ground)	203 ± 1.6	101 ± 2.4	261 ± 4.0	107 ± 0.76	128
Sample 2 (1 g/50 mL)	431 ± 2.1	95 ± 1.3	358 ± 7.4	115 ± 1.7	83
Sample 2 (2 g/50 mL)	440 ± 0.89	96 ± 4.0	498 ± 140	172 ± 17	113
CRM	296 ± 1.9	90 ± 3.3	274 ± 3.8	151 ± 8.1	92
Certificate (320 ± 31 mg kg^{-1})	Recovery 92.6 ± 0.59%		Recovery 85.7 ± 1.2%		

method for determination of fluoride in tea) the nICPMS results showed differences without any recognizable trend due to the low number of samples (Table 3).

In principle the system is useable as it is when the fluorine concentration in the samples to be measured is about 0.1 mg L^{-1} or higher. The influence of the matrix, especially high cation load and carbon, must be studied before wider applications are considered. Also efforts should be made to find a suitable internal standard element to minimise matrix effects, nebulization and plasma loading effects. The signal at m/z 18 may be a potential candidate for internal standardisation as may be others. A study about the influence of major matrix elements on signal intensity in nICPMS is still required. In principle m/z 18 would be an ideal candidate for internal standardisation, since it is under wet plasma conditions present at near constant amounts in every solution introduced into the system.

4. Conclusion

Negative ion ICPMS (nICPMS) is in principle a suitable technique for the determination of halogens, especially fluorine. For now, detection limits for fluorine are similar to those achieved using the BaF^+ in positive-ion ICPMS. To achieve better detection limits the interface region of the instrument and its influence on signal intensity need to be explored in more detail. Since the ionisation of halogen atoms in nICPMS takes place in the interface and not in the plasma, potential improvements to the interface should be explored in the future. At the moment the design of the interface region is based purely on the requirements for positive ions in pICPMS. Whether changes in the interface to improve the sensitivity of negative ions would remain compatible with positive ion detection and therefore allow the construction of an instrument capable of measuring in both modes needs further studies.

Another major stumbling block to achieving good detection limits for halogens is the widespread contamination of solvents and the laboratory environment with halogens. The high fluorine background has already been recognised when pICPMS, CIC or HR GFMAS were used.[15,18] Therefore, the identification of fluorine sources and their elimination is mandatory for the development of a sensitive fluorine-specific detector of any type.

nICPMS, as is, can be applied for the detection of halogens in samples or used as a detector for single particles, laser ablation or chromatography taking the relatively high l.o.d. into account. However, before widespread application the influence of other ions on signal intensity and stability should be tested and attempts should be made to identify a suitable internal standard.

Data availability

The data supporting this article have been included as part of the ESI† (raw data Raab *et al.* JAAS 2025.zip).

Author contributions

Andrea Raab was responsible for the experiments and writing of the draft. Jörg Feldmann and Hamid Badiei contributed to writing and critical discussions.

Conflicts of interest

There are no conflicts to declare.

Acknowledgements

We acknowledge Bohdan Atamanchuk for his assistance with the development of the detector and its electronics and Bill Fisher at PerkinElmer Scientific Canada ULC for his support. We acknowledge the University of Graz for financial support to publish this work as an open access paper.

References

1 H. Fiedler, T. Kennedy and B. J. Henry, *Integr. Environ. Assess. Manag.*, 2021, **17**, 331–351.
2 B. M. Johnson, Y.-Z. Shu, X. Zhuo and N. A. Meanwell, *J. Med. Chem.*, 2020, **63**, 6315–6386.
3 D. Chiodi and Y. Ishihara, *J. Med. Chem.*, 2023, **66**, 5305–5331.
4 R. A. Brase, E. J. Mullin and D. C. Spink, *Int. J. Mol. Sci.*, 2021, **22**, 995.
5 L. A. Schaider, S. A. Balan, A. Blum, D. Q. Andrews, M. J. Strynar, M. E. Dickinson, D. M. Lunderberg, J. R. Lang and G. F. Peaslee, *Environ. Sci. Technol. Lett.*, 2017, **4**, 105–111.
6 IARC, Some Inorganic Substances, Chlorinated Hydrocarbons, Aromatic Amines, N-Nitroso Compounds, and Natural Products, *IARC Monographs on the Evaluation of Carcinogenic Risks to Humans*, World Health Organization, Geneva, 1972.

7 R. Aro, U. Eriksson, A. Kärrman and L. W. Y. Yeung, *Environ. Sci. Technol.*, 2021, **55**, 13142–13151.
8 K. M. Spaan, B. Yuan, M. M. Plassmann, J. P. Benskin and C. A. de Wit, *Environ. Sci. Technol.*, 2023, **57**, 9309–9320.
9 L. A. D'Agostino and S. A. Mabury, *Environ. Sci. Technol.*, 2014, **48**, 121–129.
10 W. Xu, X. Wang and Z. Cai, *Anal. Chim. Acta*, 2013, **790**, 1–13.
11 A. Dreyer, I. Weinberg, C. Temme and R. Ebinghaus, *Environ. Sci. Technol.*, 2009, **43**, 6507–6514.
12 D. J. Muensterman, L. Cahuas, I. A. Titaley, C. Schmokel, F. B. de La Cruz, M. A. Barlaz, C. C. Carignan, G. F. Peaslee and J. A. Field, *Environ. Sci. Technol. Lett.*, 2022, **9**, 320–326.
13 J. Feldmann, A. Raab and E. M. Krupp, *Anal. Bioanal. Chem.*, 2018, **410**, 661–667.
14 D. K. Oliveira, V. H. Cauduro, E. L. Moraes Flores and E. M. M. Flores, *Anal. Chim. Acta*, 2024, **1288**, 342054.
15 Z. Qin, D. McNee, H. Gleisner, A. Raab, K. Kyeremeh, M. Jaspars, E. Krupp, H. Deng and J. Feldmann, *Anal. Chem.*, 2012, **84**, 6213–6219.
16 M. Resano and E. García-Ruiz, *Anal. Bioanal. Chem.*, 2011, **399**, 323–330.
17 B. Welz, S. Morés, E. Carasek, M. G. R. Vale, M. Okruss and H. Becker-Ross, *Appl. Spectro. Rev.*, 2010, **45**, 327–354.
18 N. L. A. Jamari, J. F. Dohmann, A. Raab, E. M. Krupp and J. Feldmann, *J. Anal. At. Spectrom.*, 2017, **32**, 942–950.
19 N. Yamada, *Agilent Applications Handbook*, 2015, vol. 2.
20 W. Guo, L. Jin, S. Hu and Q. Guo, *J. Agric. Food Chem.*, 2017, **65**, 3406–3412.
21 B. Lajin and W. Goessler, *Anal. Chim. Acta*, 2020, **1094**, 11–17.
22 W. Guo, X. Lin, L. Jin and S. Hu, *J. Food Compos. Anal.*, 2020, **86**, 103378.
23 A. M. Schwan, R. Martin and W. Goessler, *Anal. Methods*, 2015, **7**, 9198–9205.
24 X. Bu, T. Wang and G. Hall, *J. Anal. At. Spectrom.*, 2003, **18**, 1443.
25 Y. Okamoto, *J. Anal. At. Spectrom.*, 2001, **16**, 539–541.
26 P. Maung and D. Beauchemin, *J. Anal. At. Spectrom.*, 2020, **35**, 1097–1102.
27 M. M. Bayon, A. R. Garcia, J. I. Alonso and A. Sanz-Medel, *Analyst*, 1999, **124**, 27–31.
28 C. Brede, E. Lundanes, T. Greibrokk, S. Pedersen-Bjergaard and H. R. C.-J. High, *Res. Chrom.*, 1998, **21**, 282–286.
29 C. Brede, S. Pedersen-Bjergaard, E. Lundanes and T. Greibrokk, *J. Anal. At. Spectrom.*, 2000, **15**, 55–60.
30 J. E. Lesniewski, W. P. McMahon and K. Jorabchi, *J. Anal. At. Spectrom.*, 2018, **33**, 1981–1992.
31 J. E. Lesniewski, K. Zheng, P. Lecchi, D. Dain and K. Jorabchi, *Anal. Chem.*, 2019, **91**, 3773–3777.
32 F. A. Redeker, J. E. Lesniewski, G. Hahm, W. P. McMahon and K. Jorabchi, *Anal. Chem.*, 2022, **94**, 11865–11872.
33 G. H. Vickers, D. A. Wilson and G. M. Hieftje, *Anal. Chem.*, 1988, **60**, 1808–1812.
34 J. E. Fulford and E. S. Quan, *Appl. Spectro.*, 1988, **42**, 425–428.
35 M. Chtaib and J. P. Schmit, *J. Anal. At. Spectrom.*, 1988, **3**, 315–318.
36 M. Chisum, *Atom. Spectro.*, 1991, **12**, 155–159.
37 A. Pupyshev and V. Surikov, *Spectrochim. Acta, Part B*, 2004, **59**, 1021–1031.
38 S. Canulescu, I. S. Molchan, C. Tauziede, A. Tempez, J. A. Whitby, G. E. Thompson, P. Skeldon, P. Chapon and J. Michler, *Anal. Bioanal. Chem.*, 2010, **396**, 2871–2879.
39 N. K. Sugiyama N, *Agilent Technical Note*.
40 G. Horlick, S. H. Tan, M. A. Vaughan and C. A. Rose, *Spectrochim. Acta Part B*, 1985, **40**, 1555–1572.
41 N. L. A. Jamari, A. Behrens, A. Raab, E. M. Krupp and J. Feldmann, *J. Anal. At. Spectrom.*, 2018, **33**, 1304–1309.
42 N. L. A. Jamari, J. F. Dohmann, A. Raab, E. M. Krupp and J. Feldmann, *Anal. Chim. Acta*, 2019, **1053**, 22–31.
43 *Directive (EU) 2020/2184*, **https://eur-lex.europa.eu/legal-content/en/TXT/?uri=CELEX%3A32020L2184**.
44 Y. Zhu, K. Nakano and Y. Shikamori, *Anal. Sci.*, 2017, **33**, 1279–1284.
45 B. Lajin and W. Goessler, *Anal. Chem.*, 2020, **92**, 9156–9163.
46 S. Dubascoux, D. Andrey, M. Vigo, P. Kastenmayer and E. Poitevin, *J. Trace Elem. Med. Biol.*, 2018, **49**, 19–26.
47 H. Niu and R. S. Houk, *Spectrochim. Acta Part B*, 1996, **51**, 779–815.
48 R. E. Good, *NASA CR-516*, 1966.
49 N. Kivel, H.-D. Potthast, I. Günther-Leopold, F. Vanhaecke and D. Günther, *Spectrochim. Acta Part B*, 2014, **93**, 34–40.
50 N. Taylor and P. B. Farnsworth, *Spectrochim. Acta Part B*, 2012, **69**, 2–8.
51 H. S. NIU and R. S. Houk, *Spectrochim. Acta Part B y*, 1994, **49**, 1283–1303.
52 H. B. Lim, R. S. Houk, M. C. Edelson and K. P. Carney, *J. Anal. At. Spectrom.*, 1989, **4**, 365.
53 K. Nagulin, I. V. Tsivilskiy, D. Akhmetshin and A. Gilmutdinov, *Spectrochim. Acta Part B*, 2017, **135**, 63–72.
54 S. Canulescu, J. Whitby, K. Fuhrer, M. Hohl, M. Gonin, T. Horvath and J. Michler, *J. Anal. At. Spectrom.*, 2009, **24**, 178–180.
55 E. Stoffels, W. W. Stoffels and K. Tachibana, *Rev. Sci. Instrum.*, 1998, **69**, 116–122.
56 E. Stoffels, W. W. Stoffels, D. Vender, M. Haverlag, G. M. W. Kroesen and F. J. de Hoog, *Contrib. Plasma Phys.*, 1995, **35**, 331–357.
57 M. A. Huels, J. A. Fedchak, R. L. Champion, L. D. Doverspike, J. P. Gauyacq and D. Teilletbilly, *Phys. Rev. A*, 1994, **49**, 255–264.
58 W. W. Stoffels, E. S. Eva Stoffels and K. T. Kunihide Tachibana, *Jpn. J. Appl. Phys.*, 1997, **36**, 4638.
59 H. B. Lim and R. S. Houk, *Spectrochim. Acta Part B*, 1990, **45**, 453–461.
60 J. E. Fulford and D. J. Douglas, *Appl. Spectro.*, 1986, **40**, 971–974.
61 H. B. Lim, R. S. Houk and J. S. Crain, *Spectrochim. Acta Part B*, 1989, **44**, 989–998.